J|A|C|S COMMUNICATIONS

Published on Web 01/05/2010

Curvature Sensing by the Epsin N-Terminal Homology Domain Measured on Cylindrical Lipid Membrane Tethers

Benjamin R. Capraro,[†] Youngdae Yoon,[‡] Wonhwa Cho,[‡] and Tobias Baumgart*[,†]

Department of Chemistry, University of Pennsylvania, Philadelphia, Pennsylvania 19104, and Department of Chemistry, University of Illinois at Chicago, Chicago, Illinois 60607

Received September 23, 2009; E-mail: baumgart@sas.upenn.edu

The protein epsin is believed to play important roles in clathrin-mediated endocytosis, including generation of the high membrane curvature necessary for vesicle formation.[1−3] Evidence for this hypothesis comes, in part, from electron microscopy observations of liposomes deformed into tubules when incubated with epsin or epsin N-terminal homology (ENTH) domain in purified form.[3] However, vesicle cosedimentation showed ENTH membrane binding independent of liposome curvature radius,[4] thus shedding no light on the mechanism of ENTH membrane tubulation.

Here we have systematically quantified the curvature dependence of epsin ENTH area density on cylindrical membranes with controlled curvature. We have observed repartitioning of membrane-bound ENTH from a quasi-flat membrane area and protein reservoir onto highly curved membranes and obtained the first measurement of Leibler's[5] thermodynamic curvature−composition coupling coefficient, Λ, for an endocytic accessory protein.

Epsin is involved with multiple intracellular trafficking processes,[6] and in clathrin-mediated endocytosis, it aids in cargo selection and links the membrane to other proteins involved in vesicle formation before proteins such as dynamin accomplish fission.[1,7] Studies of epsin's conserved membrane-contacting ENTH domain[8] have suggested a molecular rationale for the role of epsin in curvature sensing and generation, demonstrating its high affinity for the phosphoinositide PIP_2[3,8,9] coupled with membrane insertion of the N-terminal helix.[9,10]

To be able to mechanically understand cellular membrane deformation processes, identifying and characterizing roles for proteins in the generation and sensing of membrane curvature is required.[1] Sensitive methods must be applied to quantify these phenomena. Such measurements, when compared with high-resolution structural, spectroscopic, and simulation data, will also allow us to relate molecular descriptions of interactions to macroscopic membrane remodeling in cells.[11]

Here we used a recently developed approach to quantify the partitioning in membrane curvature gradients of peripherally binding proteins.[12−14] Connected membrane regions differing in curvature by orders of magnitude were obtained by micropipet-assisted pulling of cylindrical tethers[15] from giant unilamellar vesicles (GUVs), and partitioning of membrane components between the high-curvature tether and the low-curvature vesicle was measured by fluorescence microscopy.[12,13]

We monitored fluorescence from an ENTH−green fluorescent protein chimera bound to individual tethers of palmitoyloleoylphosphatidylcholine (POPC) membranes doped with PIP_2 under different levels of membrane tension, σ, controlled by micropipet aspiration. The tether radius depends on membrane tension in an inverse-square-root relationship.[12] We have shown previously that tether fluorescence obeys a linear dependence on measured tether radius for membrane fluorophores without curvature preference.[13] Therefore, the null hypothesis of curvature-independent binding would predict ENTH−GFP fluorescence to *decrease* as σ is increased.

Contrarily, we observed that green (protein) fluorescence from the tether markedly *increased* at high σ (compare panels A and C of Figure 1), whereas red (lipid) fluorescence became dimmer, reflecting tension-induced narrowing of the tether (Figure 1B,D).

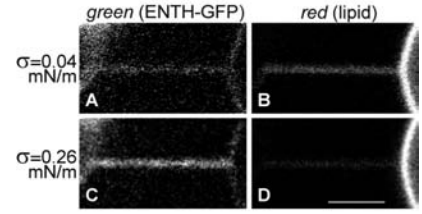

Figure 1. Curvature partitioning of ENTH−GFP on tubular membranes. A membrane tether (with diameter controllable to within ∼25−140 nm) was formed from a micropipet-aspirated 1 mol % PIP_2-containing POPC GUV (at the right) by means of a polystyrene bead (visible on the left in the green channel) held with a second micropipet and imaged by confocal fluorescence microscopy. (A, C) Green channel detecting ENTH−GFP fluorescence. (B, D) Red channel detecting Texas Red (TR) fluorescence from TR−DHPE. (A, B) Simultaneously collected images at low membrane tension (σ = 0.039 mN/m); (C, D) σ = 0.259 mN/m. Scale bar: 3 μm.

Thus, as the curvature is increased, ENTH molecules repartition to the tether region of the membrane.

To enable quantitation of ENTH curvature coupling [Figure 2A and Figure S1 in the Supporting Information (SI)], we measured the Kalman-averaged fluorescence intensity in confocal microscopy imaging planes orthogonal (*xz* plane) to the tether symmetry axis (lying in the *xy* plane). The ratio of protein and lipid [Texas Red (TR)−DHPE] fluorescence intensities, $I_r = I_{green}/I_{red}$, served as a metric of curvature partitioning and was shown to increase with σ (Figure 2B; also see the SI). In particular, an essentially linear dependence of I_r on $\sigma^{1/2}$ was observed (Figure 2B), in accordance with a first-order thermodynamic theory (see below).

We quantitatively assessed the reversibility and time scale of equilibration of fluorescence changes in response to σ changes (Figure 2C,D), verifying that I_r stabilizes soon (<1 min) following σ increases and reverses following σ lowerings (Figure 2D). These findings justify our adaptation of thermodynamic theory to determine the coupling parameter Λ for ENTH curvature partitioning (also see the SI).

Specifically, we related measured fluorescence to local concentration changes, considering the associated entropy of lipid mixing as being offset by the unique tendency of ENTH to translocate to regions of high curvature. Fluorescence intensity ratios I_r were normalized with the value of I_r^0 obtained from extrapolation to zero curvature of linear fits of I_r versus $\sigma^{1/2}$ (Figure 2E, all equilibration times chosen as ∼1 min).

Individually normalized data sets were binned (Figure 2F) and fitted with eq 1:

[†] University of Pennsylvania.
[‡] University of Illinois at Chicago.

10.1021/ja907936c

$$\frac{I_r}{I_r^0} = 1 + \frac{\Delta\phi}{\phi_v} = 1 - \frac{\Lambda}{\rho kT}\sqrt{\frac{2\sigma}{\kappa_{eff}}} \quad (1a)$$

$$\kappa_{eff} = \kappa_0 - \Lambda^2\chi \quad (1b)$$

where $\Delta\phi$ is the PIP_2 mole fraction difference between the tether and the vesicle mole fraction ϕ_v, κ_0 and κ_{eff} are the bare and renormalized membrane bending stiffnesses, respectively, $\chi = \phi_v/\rho kT$ is the osmotic compressibility (here approximated as for an ideal gas of membrane-bound proteins), k is Boltzmann's constant, and ρ is the lipid density. The fit yielded $\Lambda = -146 \pm 3$ pN for the data for POPC/1 mol % PIP_2 membranes presented in Figure 2F. Equation 1 quantifies curvature sensing as a function of the molecular property Λ in eq 1a and curvature generation as a function of Λ *and* the concentration of curvature generators (ϕ_v, assuming that PIP_2 is ENTH-saturated with 1:1 binding stoichiometry[3]) through softening of the bare stiffness in eq 1b. It should be noted that curvature sensing is amplified with increasing ϕ_v at constant Λ.

Our analysis assumes that PIP_2 itself does not possess appreciable membrane curvature preference, which follows from our measurements on tethers containing a fluorescent PIP_2 analogue (Figure S2). Evidence supporting our additional assumption of the equilibration of ENTH chemical potentials on the vesicle and tube was provided by time-lapse imaging following a tension jump (Figure S3). A front of green fluorescence emerged from the vesicle and advanced on the tether (equilibration times <1 min), revealing also that ENTH molecules relocate onto the tether membrane from the vesicle rather than from aqueous solution.

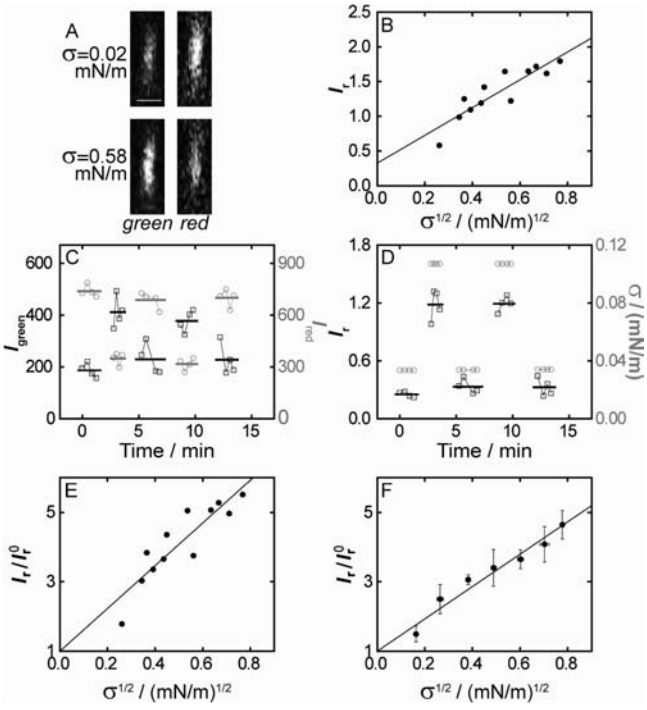

Figure 2. Curvature dependence of ENTH membrane localization. (A) Demonstration of Kalman-averaged confocal *xz* line-scan images (obtained near the tether base) used to monitor ENTH−GFP binding under varying tension. Bar: 1 μm. (B) Plot of the ratio of green and red channel fluorescence intensities ($I_r = I_{green}/I_{red}$) from images typified in (A) (see the SI) as a function of the square root of membrane tension for an individual tether, revealing a linear relationship. The line shows a linear fit with intercept $I_r^0 = 0.33 \pm 0.17$. (C) Demonstration of reversibility and equilibration under the conditions as used in (A) and (B). Green and red intensities for two cyclic tension changes [tension values in (D)]. Left axis, black squares, I_{green}; right axis, gray circles, I_{red}. Bold lines indicate average fluorescence values from four images for each σ. (D) I_r values for the data in (C) (left axis, black squares), with indicated tension levels (right, gray circles). (E) I_r values from (B) were normalized to I_r^0 and fitted using eq 1 (see the SI), yielding $\Lambda = -169 \pm 4$ pN (the uncertainty is from linear regression). (F) Data from seven vesicles processed as demonstrated in (B) and (E) were binned (error bars represent standard errors of the mean) and fitted with eq 1, yielding $\Lambda = -146 \pm 3$ pN (uncertainty from regression).

Elasticity theory predicts curvature generation[16] based on membrane insertion of ENTH's N-terminal helix.[9] However, an inability to tubulate liposomes despite established amphipathic insertion was observed for some peripherally binding proteins,[17] highlighting the possibility that additional parameters, such as lipid composition and protein oligomerization, may contribute to membrane deformation by proteins. Future research probing curvature-dependent binding by our method, when compared with characterization of insertion and tubulation, will aid in the attribution of functional membrane deformation to particular proteins in addition to the elucidation of the underlying mechanisms.

Using membrane tethers incubated with ENTH, we occasionally observed structures reminiscent of the "focal swellings" described in dynamin-bound membrane tubules.[18] In bead-shaped regions of lower curvature coexisting with the tether, ENTH was conspicuously depleted (Figure S4), echoing the curvature partitioning between tether and vesicle and hinting at interesting mechanical instabilities induced by epsin.

In summary, we have reported the first experimental measurement of a negative curvature−composition coupling constant for a membrane-binding protein. Our results demonstrate that ENTH binds preferentially to highly curved membranes, highlighting the possibility that it contributes to cellular membrane curvature sensing and generation.

Acknowledgment. Funding came from NSF Grant MCB-0718569 and the Alfred P. Sloan Foundation.

Supporting Information Available: Materials and methods and supporting figures. This material is available free of charge via the Internet at http://pubs.acs.org.

References

(1) Doherty, G. J.; McMahon, H. T. *Annu. Rev. Biochem.* **2009**, *78*, 857.
(2) Itoh, T.; Koshiba, S.; Kigawa, T.; Kikuchi, A.; Yokoyama, S.; Takenawa, T. *Science* **2001**, *291*, 1047.
(3) Ford, M. G.; Mills, I. G.; Peter, B. J.; Vallis, Y.; Praefcke, G. J.; Evans, P. R.; McMahon, H. T. *Nature* **2002**, *419*, 361.
(4) Peter, B. J.; Kent, H. M.; Mills, I. G.; Vallis, Y.; Butler, P. J.; Evans, P. R.; McMahon, H. T. *Science* **2004**, *303*, 495.
(5) Leibler, S. *J. Phys. (Paris)* **1986**, *47*, 507.
(6) Wendland, B. *Nat. Rev. Mol. Cell. Biol.* **2002**, *3*, 971.
(7) Legendre-Guillemin, V.; Wasiak, S.; Hussain, N. K.; Angers, A.; McPherson, P. S. *J. Cell. Sci.* **2004**, *117*, 9.
(8) Itoh, T.; De Camilli, P. *Biochim. Biophys. Acta* **2006**, *1761*, 897.
(9) Stahelin, R. V.; Long, F.; Peter, B. J.; Murray, D.; De Camilli, P.; McMahon, H. T.; Cho, W. *J. Biol. Chem.* **2003**, *278*, 28993.
(10) Hom, R. A.; Vora, M.; Regner, M.; Subach, O. M.; Cho, W.; Verkhusha, V. V.; Stahelin, R. V.; Kutateladze, T. G. *J. Mol. Biol.* **2007**, *373*, 412.
(11) McMahon, H. T.; Gallop, J. L. *Nature* **2005**, *438*, 590.
(12) Sorre, B.; Callan-Jones, A.; Manneville, J. B.; Nassoy, P.; Joanny, J. F.; Prost, J.; Goud, B.; Bassereau, P. *Proc. Natl. Acad. Sci. U.S.A.* **2009**, *106*, 5622.
(13) Tian, A.; Baumgart, T. *Biophys. J.* **2009**, *96*, 2676.
(14) Tian, A.; Capraro, B. R.; Esposito, C.; Baumgart, T. *Biophys. J.* **2009**, *97*, 1636.
(15) Hochmuth, R. M.; Wiles, H. C.; Evans, E. A.; McCown, J. T. *Biophys. J.* **1982**, *39*, 83.
(16) Campelo, F.; McMahon, H. T.; Kozlov, M. M. *Biophys. J.* **2008**, *95*, 2325.
(17) Cho, W.; Stahelin, R. V. *Annu. Rev. Biophys. Biomol. Struct.* **2005**, *34*, 119.
(18) Roux, A.; Uyhazi, K.; Frost, A.; De Camilli, P. *Nature* **2006**, *441*, 528.

JA907936C